Steady-state *ab initio* laser theory for fully or nearly degenerate cavity modes

Stephan Burkhardt, Matthias Liertzer, Dmitry O. Krimer, and Stefan Rotter
Institute for Theoretical Physics, Vienna University of Technology, Wiedner Hauptstraβe 8-10/136, A-1040 Vienna, Austria
(Received 12 March 2015; published 27 July 2015)

We investigate the range of validity of the recently developed steady-state *ab initio* laser theory (SALT). While very efficient in describing various microlasers, SALT is conventionally believed not to be applicable to lasers featuring fully or nearly degenerate pairs of resonator modes above the lasing threshold. Here we demonstrate how SALT can indeed be extended to describe such cases as well, with the effect that we significantly broaden the theory's scope. In particular, we show how to use SALT in conjunction with a linear stability analysis to obtain stable single-mode lasing solutions that involve a degenerate mode pair. Our flexible and efficient approach is tested on one-dimensional ring lasers as well as on two-dimensional microdisk lasers with broken symmetry.

DOI: 10.1103/PhysRevA.92.013847 PACS number(s): 42.55.Ah, 42.65.Sf, 42.55.Sa

I. INTRODUCTION

Microcavity lasers are essential elements in modern photonics and have been realized with cavities of very different shape and with various lasing mechanisms [1–12]. The nonlinear lasing behavior of these systems can, in principle, be modeled using the semiclassical Maxwell-Bloch (MB) equations [13–16]. Due to their time-dependent nature these equations are, however, usually difficult to solve for all but the most simple cases. In recent years, a much more efficient approach named steady-state *ab initio* lasing theory (SALT) has emerged, which can be used to describe the steady-state lasing of lasers [17–23]. Among other advances, this framework has shed light on weakly scattering random lasers [24], on pump-induced exceptional points [11,12,25,26], and on coherent perfect absorption [27,28] and has opened up ways of controlling the emission patterns of random as well as of microcavity lasers [29,30]. One of the major drawbacks of SALT is that its conventional formulation fails for the simulation of microlasers with nearly degenerate modes as occurring, e.g., in whispering gallery mode resonators with an inherent symmetry [2,6,8,10,12,31].

Here, we present an approach to generalize SALT to such cases. This extension allows us to observe, among other phenomena, that nearly degenerate modes may merge into a single mode. These steady-state solutions are, however, not necessarily stable with respect to small time-dependent spatial perturbations. In particular, it has already been shown that in highly symmetric systems such as ring lasers not every steady-state solution of the MB equations is necessarily stable [32,33]. Hence, the stability of the solutions obtained from our extended SALT approach has to be verified. Up to now such additional stability checks were always done using direct time-dependent simulations of the MB equations [18,25,34,35]. One of the reasons for using SALT, however, is exactly to avoid this kind of computationally very demanding numerics.

In this work, we thus introduce a much more efficient way to determine the stability of the SALT solutions based on a rigorous linear stability analysis for single-mode steady-state solutions. Furthermore, our work extends the scope of SALT to previously inaccessible parameter regimes, where even bifurcating solutions (stable or unstable) of the nonlinear equations can now be appropriately dealt with.

II. SHORT REVIEW OF SALT

In semiclassical laser theory, the dynamics of a laser is governed by the interaction of classical fields with an ensemble of two-level atoms as described by the so-called Maxwell-Bloch (MB) equations. Restricting the fields to one dimension or to the transverse magnetic (TM) polarization in two dimensions, the electric field and polarization become scalar [36]. Using the rotating wave approximation, the MB equations can be derived as follows [16]:

$$\begin{aligned} \epsilon \ddot{E}^+ &= \nabla^2 E^+ - \ddot{P}^+, \\ \dot{P}^+ &= -(i\omega_a + \gamma_\perp)P^+ - i\gamma_\perp E^+ D, \\ \frac{\dot{D}}{\gamma_\parallel} &= D_0 - D + \frac{i}{2}[E^+(P^+)^* - \text{c.c.}]. \end{aligned} \tag{1}$$

In these nonlinear partial differential equations, $E^+(x,t)$ and $P^+(x,t)$ denote the positive frequency components of the electrical field and the polarization of the medium, respectively. The quantity $D(x,t)$ is the population inversion of the two-level atoms and $D_0(x)$ stands for the externally imposed pump strength. The constants in the MB equations describe the properties of the cavity and of the gain material: the dielectric function $\epsilon(x)$, the transition frequency of the two-level atoms ω_a, as well as the decay rates of the polarization $\gamma_\perp$ and of the population inversion $\gamma_\parallel$. The boundary conditions for the equations above are typically outgoing boundary conditions, which numerically can, e.g., be implemented using a perfectly matched layer [22,37].

The natural units in Eqs. (1) and all example systems in this work can be converted back to SI units by choosing an appropriate length scale $\tilde{L}$, multiplying all lengths in the example systems by this quantity $\tilde{L}$, multiplying the quantities $(\frac{\partial}{\partial t},\gamma_\parallel,\gamma_\perp,\omega_a)$ by $c/\tilde{L}$, where c is the speed of light, dividing $\frac{\partial}{\partial x}$ by $\tilde{L}$, and finally by transforming E, P, and D as follows: $E^+_{\text{SI}} = E^+ \frac{2g}{\hbar\sqrt{\gamma_\parallel\gamma_\perp}} \equiv E^+ e_{\text{SI}}$, $P^+_{\text{SI}} = P^+ \frac{2g}{\hbar\epsilon_0\sqrt{\gamma_\parallel\gamma_\perp}}$, and $D_{\text{SI}} = D\frac{g^2}{\hbar\gamma_\perp\epsilon_0}$. The variable g is the transition dipole moment of the two-level atoms.

For microlaser systems lasing in steady state, only a finite number of modes in the system are active. This is the case described by SALT, in which the MB equations are simplified to a set of time-independent, non-Hermitian, nonlinear, and coupled Helmholtz equations. The solutions of these SALT

equations are much more efficiently calculated than those of the MB equations [18,25,34,35].

The cornerstone of the SALT equations is a multiperiodic ansatz for the electromagnetic field as well as for the polarization

$$E^+(x,t) = \sum_{\mu=1}^{N} E_\mu(x)\, e^{-i\omega_\mu t},$$
$$P^+(x,t) = \sum_{\mu=1}^{N} P_\mu(x)\, e^{-i\omega_\mu t}, \tag{2}$$

where each triplet $(E_\mu, P_\mu, \omega_\mu)$ represents a mode E_μ of the system lasing at the *real* frequency ω_μ. Inserting the ansatz (2) into the last equation of (1) results in

$$\dot{D} = \gamma_\parallel (D_0 - D) + \frac{i\gamma_\parallel}{2} \sum_{\mu,\nu} (E_\mu P_\nu^* e^{i(\omega_\nu - \omega_\mu)t} - \text{c.c.}) \tag{3}$$

with terms of the form $P_\nu E_\mu^* e^{i(\omega_\nu - \omega_\mu)t}$, which explicitly depend on time. For multiple lasing modes, D will thus never be completely static. However, if the time scale $1/(\omega_\nu - \omega_\mu)$ on which these terms oscillate is much shorter than the time scale on which D varies $(1/\gamma_\parallel)$, their contribution can be neglected. In other words, for systems where $\Delta\omega = |\omega_\nu - \omega_\mu| \gg \gamma_\parallel$ holds for all pairs μ,ν of active modes [38] the inversion can be approximated to be stationary [17,22].

This stationary inversion approximation (SIA) is, however, not well satisfied in macroscopic lasers with a large density of modes as well as in microcavity lasers with an inherent symmetry. We will focus here on the latter case and shall consider ring or microdisk lasers with degenerate modes or slightly perturbed versions of these systems with nearly degenerate modes. The frequency splitting of these nearly degenerate modes will typically violate the condition $\Delta\omega \gg \gamma_\parallel$ for realistic values of $\gamma_\parallel$. Since not only the lasing frequencies of these modes are very close to each other but also their thresholds are at comparable pump strengths D_0, the traditional SALT algorithm will not be applicable when both modes of such a pair move across the lasing threshold. For the completely degenerate case this problem is even more acute.

In the following, we will provide an extension of the SALT algorithm, which is able to overcome this significant drawback. Our extension takes into account that degenerate modes with a fixed relative phase can be expressed as a single active lasing mode within the SALT formalism. For nearly degenerate modes, we find that such a mode pair can become dynamically stable in the form of a single lasing mode, allowing us to treat the solution again with the above SALT ansatz. In order to present our approach as clearly as possible, we will focus here on the case of single-mode lasing only, keeping in mind that our algorithm can be generalized to multiple pairs of degenerate modes or multiple modes in general [39].

For a single lasing mode the ansatz (2) satisfies the MB Eqs. (1) exactly, leading to the following single-mode SALT equation for the electric field E_1 and for the *real* lasing frequency ω_1:

$$\left[\nabla^2 + \left(\epsilon(x) + \Gamma_1 \frac{D_0(x)}{1 + |\Gamma_1 E_1(x)|^2}\right)\omega_1^2\right] E_1(x) = 0, \tag{4}$$

where

$$\Gamma_1 = \frac{\gamma_\perp}{\omega_1 - \omega_a + i\gamma_\perp}, \tag{5}$$

and the boundary conditions are the same as for the MB equations. Note that Eq. (4) depends nonlinearly both on the frequency ω_1 as well as on the shape of the mode $E_1(x)$ through a self-saturation spatial hole burning interaction. It can be straightforwardly solved using a Newton-Raphson solver as described in detail in [22]. The solver requires an initial guess which can be obtained by tracking the modes in the system from an initial value at zero pump strength up to the pump strength of interest. This procedure has the advantage that for small pump values (below the lasing threshold) one can use the following eigenvalue problem that is linear with respect to the mode profiles:

$$\left(\nabla^2 + [\epsilon(x) + \bar{\Gamma}_i\, D_0(x)]\bar{\omega}_i^2\right)\bar{E}_i(x) = 0, \tag{6}$$

where $\bar{\Gamma}_i = \gamma_\perp/(\bar{\omega}_i - \omega_a + i\gamma_\perp)$. (Note that we label all quantities below the lasing threshold by overbars.) For pump strength $D_0 = 0$ the complex eigenvalues $\bar{\omega}_i$ have a negative imaginary part. When increasing the pump strength, the eigenfrequencies will typically move towards the real axis (interesting exceptions to this rule are discussed in [11,12,25]). Once the first eigenvalue $\bar{\omega}_1$ crosses the real axis (we assume its index i is 1) it can be used as a guess for solving Eq. (4) for the first lasing mode E_1 with real frequency ω_1. This solution can then be tracked to even higher pump strengths beyond the lasing threshold by repeatedly solving Eq. (4) for increasing D_0 while using the solution from the previous step as an initial guess. Alternative methods to solve Eq. (4) based on an expansion of laser modes in a biorthogonal basis of "constant-flux states" [17] work in a similar way but will not be considered here.

In the traditional SALT algorithm the validity of a single-mode solution $\{E_1,\omega_1\}$ of Eq. (4) is only indirectly assessed by keeping track of the remaining passive modes of the system. While only one mode $\{E_1,\omega_1\}$ is lasing all these other modes (with $i \neq 1$) have to solve the following nonlinear, non-Hermitian eigenvalue problem:

$$\left[\nabla^2 + \left(\epsilon(x) + \bar{\Gamma}_i \frac{D_0(x)}{1 + |\Gamma_1 E_1(x)|^2}\right)\bar{\omega}_i^2\right] \bar{E}_i(x) = 0. \tag{7}$$

The single-mode solution is only valid as long as all other eigenmodes $\bar{E}_i$ have an eigenvalue $\bar{\omega}_i$ with imaginary part less than or equal to 0, i.e.,

$$\forall i \neq 1: \quad \text{Im}(\bar{\omega}_i) \leqslant 0. \tag{8}$$

If, however, any other of these eigenvalues crosses the real axis, the corresponding eigenmode is assumed to be active and incorporated as an additional lasing mode into the active SALT equations [22]. As long as the presence of this second lasing mode does not violate the SIA, the corresponding two-mode lasing solution is considered stable [as was previously verified using finite-difference time-domain (FDTD) simulations [18,34,35]].

As we will demonstrate through a comparison to time-dependent solutions of the MB equations, this simple criterion cannot be applied for nearly degenerate modes. In particular, we show that stable single-mode solutions may exist even

though one of the other eigenmodes in the system features an eigenvalue $\bar{\omega}_i$ with positive imaginary part. In order to be able to correctly determine the stability of a mode when using the SALT Eq. (4), we introduce below a rigorous stability criterion based on a linear stability analysis.

One of the consequences of this strategy is that eigenmodes have to be continuously tracked even when their eigenvalues cross the real axis without, however, including them as an active lasing solution. Doing this, we find that these modes exhibit complicated frequency shifts and bifurcations when varying the pump strength D_0. Examples of this kind will be discussed in the subsequent sections.

III. EXAMPLE 1: SYMMETRIC ONE-DIMENSIONAL RING LASER

To convey an understanding of how a lasing system with degenerate modes can be described in the SALT framework, let us first consider the well-known example of a rotationally symmetric ring laser whose solution can become unstable in certain parameter regimes [32,33,40–49]. We model the system as a one-dimensional (1D), homogeneous medium with periodic boundary conditions [see Fig. 1(a) for an illustration]. To incorporate losses through absorption and outcoupling, we set the index of refraction to a complex value.

Solving Eq. (6) for the unpumped system produces a set of eigenstates $\{\bar{\omega}_i, \bar{E}_i\}$, where a two-dimensional eigenspace is associated with every eigenvalue $\bar{\omega}_i$ due to the rotational symmetry of the system. This eigenspace contains standing waves of the form $e^{i\bar{\omega}_i x} \pm$ c.c. as well as traveling waves of the form $e^{\pm i\bar{\omega}_i x}$. While these two pairs of states as well as their superpositions solve Eq. (6) below threshold, the nonlinear spatial hole-burning term in the SALT Eq. (4) prevents arbitrary superpositions from being valid solutions above the threshold. The only two possible steady-state lasing solutions of the ring laser that are left at ω_i are the well-known clockwise and counterclockwise traveling-wave states. However, from the literature it is known that ring lasers show complex behavior, including the fact that these traveling-wave solutions are not always stable [32,33,40–44,46–50].

Our goal here will be to find the single-mode solutions with SALT and to identify the corresponding regions of stability. To approach this problem first in the most general way (i.e., independently of the employed SALT approach), we set up a finite-difference time-domain (FDTD) method based on a Yee lattice [51,52]. This tool allows us to solve the MB equations Eq. (1) directly, including the full temporal evolution starting from an initial distribution of the electric field [53]. Using this approach we first confirmed that in the single-mode regime indeed only the traveling modes are stable in certain parameter regimes. To assess the latter, the system was initialized in the traveling-wave solution obtained from the SALT Eq. (4) [54] and then left to evolve for a certain amount of time. We analyzed whether at later times the system remained in the same steady-state solution as at the beginning of the simulation. If the system stayed in the same state (and did not show any signatures of deviating from this state), we considered the solution to be stable.

The stability diagram resulting from these FDTD simulations is shown in Fig. 1(c). We find that the stability of

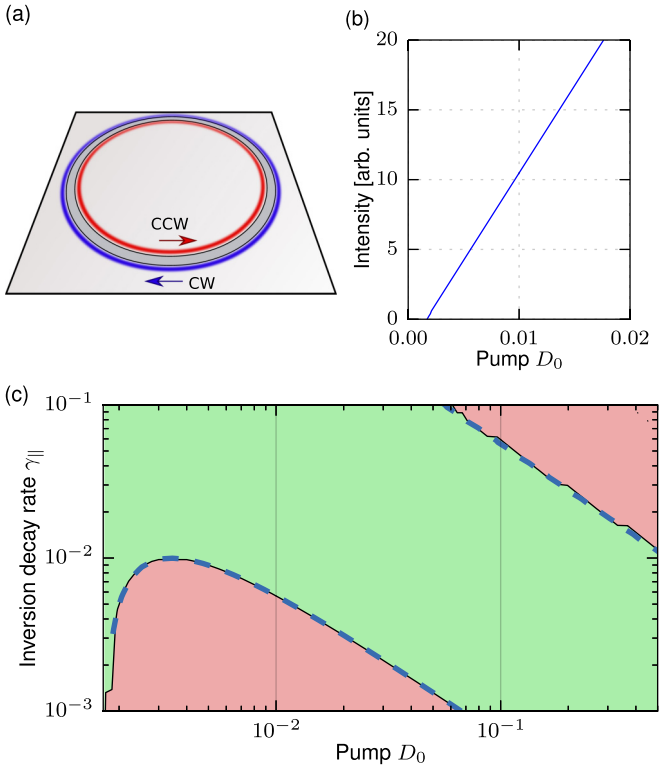

FIG. 1. (Color online) Results for a one-dimensional ring laser system with circumference $L = 1$, $\gamma_\perp = 1$, and $\omega_a = 61$. The openness of the system is modeled by a lossy dielectric function $\sqrt{\epsilon(x)} = 1 + 0.0002i$. (a) Sketch of the ring laser system, which can accommodate clockwise (CW) or counterclockwise (CCW) traveling modes. (b) Lasing mode intensity vs applied pump strength for the traveling-wave solution. Note that the gain parameters have been chosen such that only a single pair of degenerate modes reaches the lasing threshold. The traveling-wave solution in which the system lases has a frequency of $\omega \approx 62.65$ which stays constant while the pump strength is increased. (c) Stability analysis of the SALT results. Shown are the stability of this traveling-wave solution under variation of the pump strength D_0 and the relaxation rate of the inversion $\gamma_\parallel$. The results of the FDTD simulation are color coded with green (light gray) marking parameter combinations where the SALT solution is stable, whereas the red (dark gray) region represents unstable behavior and the solid black lines mark the border between those two regimes. Blue dashed lines show the independent results of the linear stability analysis, which provides an excellent estimate for the border between stable and unstable regions.

the single-mode SALT solutions not only depends on the external pump strength D_0, but also on the inversion decay rate $\gamma_\parallel$. This finding concurs with previous results [32,45] and shows that while the single-mode SALT solution is an exact solution of the MB equations, it is not necessarily a stable one. For systems with degenerate passive modes (as well as with closely spaced modes $\Delta\omega < \gamma_\parallel$ discussed below), the stability of any solution obtained from SALT is therefore not guaranteed and needs to be independently verified. Using FDTD for such a verification, as we did above, is, however, much too costly from a numerical point of view, in particular, as this would nullify the computational advantages of SALT. While the stability analysis presented in [32] for rotationally

symmetric ring lasers shows an equivalent instability for low values of both D_0 and $\gamma_\parallel$ and is computationally very cheap, it does not predict the unstable behavior observed for higher values of D_0 and $\gamma_\parallel$ parameters, as shown in Fig. 1(c) [55]. The analytic method of [32] is furthermore rather limited in scope, as it relies on the availability of exact analytic solutions for the passive modes. We will thus develop below a more general and rigorous framework to analyze the stability of SALT solutions that should be generally applicable.

IV. LINEAR STABILITY ANALYSIS

This section contains an overview of a linear stability analysis for solutions of SALT Eq. (4) (a full derivation can be found in Appendix). Our starting point is to linearize the original MB equations (1) around the SALT solution and to assess whether it is stable against small perturbations. In what follows we concentrate on the single-mode solutions only and thus insert the following expressions into the MB equations (1):

$$\begin{aligned} E(x,t) &= [E_1(x) + \delta E(x,t)]e^{-i\omega_1 t}, \\ P(x,t) &= [P_1(x) + \delta P(x,t)]e^{-i\omega_1 t}, \\ D(x,t) &= [D(x) + \delta D(x,t)]. \end{aligned} \tag{9}$$

In this ansatz, E_1, P_1, D denote, respectively, the electric field, the polarization, and the inversion of the single-mode SALT solution of Eq. (4) and δE, δP, δD are the corresponding small perturbations around it, represented by fields of the same dimension as those of the MB equations. This ansatz thus allows general perturbations on all spatial scales of all the variables present in the MB equations. Utilizing the fact that the SALT solution also exactly solves the MB equations and neglecting the higher-order contributions of the perturbations, we derive a set of linear PDEs (A3) with respect to $\delta E, \delta P, \delta D$.

As a next step we convert the resulting system of equations into a standard eigenvalue problem. A split of the complex variables into their imaginary and real parts gives rise to a set of linear equations for five independent fields, which for convenience can be represented as a single vector field, $\vec{F}(x) = (\mathrm{Re}(\delta E), \mathrm{Im}(\delta E), \mathrm{Re}(\delta P), \mathrm{Im}(\delta P), \delta D)$. We look for solutions of the form $\vec{F}(x,t) = \vec{F}(x)e^{\sigma t}$, where σ is the growth rate, and derive a set of linear equations (A6) containing the spatial dependence only. Using an appropriate discretization scheme and taking into account the periodic boundary conditions, we finally end up with a quadratic eigenvalue problem of the following form:

$$A\vec{F} + \sigma B\vec{F} + \sigma^2 C\vec{F} = 0, \tag{10}$$

where A, B, and C are the corresponding matrices whose dimensions depend on the chosen spatial discretization.

This eigenvalue problem can be solved numerically, resulting in a set of eigenvalues and eigenvectors, $\{\sigma^j, F^j(x)\}$. Note that eigenvalues with $\mathrm{Re}(\sigma^j) > 0$ stand for the perturbations, which grow exponentially in time implying that our SALT solution is unstable. Conversely, if all eigenvalues σ^j have a real part smaller than zero, the SALT solution is stable against small perturbations. Therefore, finding the eigenvalue with the largest real part is sufficient to classify the stability of the SALT solution. The imaginary part of σ stands for the frequency relative to ω_1, with which the perturbation oscillates. In Fig. 2, we show a typical example of the eigenvalue spectra $\{\sigma^j\}$ with different values of $\gamma_\parallel$ for the case of the symmetric ring laser described in the previous section. Note that due to the fact that the MB equations for the single-mode regime are invariant under a global phase rotation, the value $\sigma = 0$ always shows up. It does, however, not affect the behavior of the system and therefore is always excluded from the consideration.

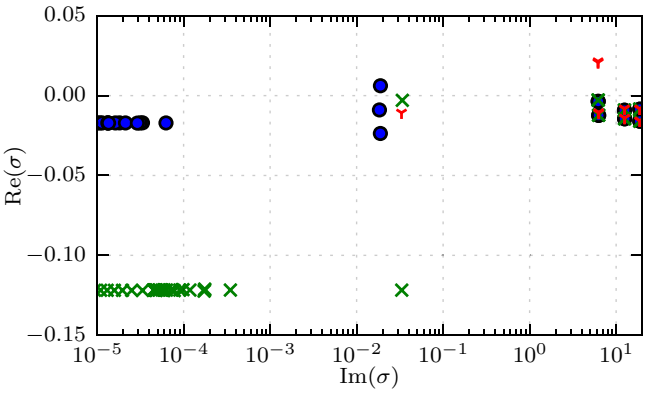

FIG. 2. (Color online) Stability eigenvalues σ^j of the ring laser for $D_0 = 0.06$ and $\gamma_\parallel = 10^{-3}$ (blue circles), $\gamma_\parallel \approx 7 \times 10^{-3}$ (green crosses), and $\gamma_\parallel = 10^{-1}$ (red Ys). All other parameters are chosen as in Fig. 1. One can see that the single-mode lasing solution is only stable for the intermediary value of $\gamma_\parallel$ (green crosses), since for both other cases, a σ^j with a real part larger than zero exists. The stability eigenvalues with $\mathrm{Im}(\sigma^j) \approx 10^{-2}$ are related to the competition between the nearly degenerate modes. The other visible clusters of stability eigenvalues at $\mathrm{Re}(\sigma^j) \approx -\gamma_\parallel$ are related to damped relaxation oscillations observed when initially turning on the laser. The eigenvalues with $\mathrm{Im}(\sigma^j) > 10$ are related to other resonances of the system that could potentially also turn into active lasing modes.

To assess the stability diagram of a SALT solution we start at a certain value of the pump strength and then gradually vary the value of $\gamma_\parallel$. The dashed lines in the stability diagram depicted in Fig. 1(c) correspond to the stability thresholds at which the eigenvalue with the largest real part, $\max_j[\mathrm{Re}(\sigma^j)]$, crosses the imaginary axis $[\mathrm{Re}(\sigma) = 0]$. We emphasize that the boundaries between stable and unstable regions, which we find in this way, are in excellent agreement with the time-dependent simulations, as seen in Fig. 1(c). It should be noted that previous studies on such a linear stability analysis involved more restrictive approximations and a limited class of perturbations by keeping track of low order Fourier terms only [32,45], whereas our approach is exact in the framework of the MB equations.

Note that for the above procedure to work it is not necessary to compute the whole eigenvalue spectrum $\{\sigma^j\}$, but it is sufficient to only consider eigenvalues in the complex region close to the real axis and for imaginary parts in the range of 0 to ω_1. In systems where the rotating wave approximation is justified, only perturbations within this frequency range can realistically influence the system. In systems with a complex refractive index, spurious solutions that need to be excluded from the analysis can occur in the region $|\mathrm{Im}(\sigma)| > \omega_1$. This restriction on the eigenvalues we are looking for can be used

together with an iterative eigenvalue solver to check relatively quickly if a solution is stable or not [56].

It is worth noting that for the above stability analysis of the MB equations no additional assumptions have been made and the results are therefore valid for arbitrary single-mode SALT solutions. In the next section we consider the ring laser with an embedded scatterer where modes are only near degenerate to see how our results change for the case of such a slight lift of the degeneracy.

V. EXAMPLE 2: 1D RING LASER WITH BROKEN SYMMETRY

In any real-world implementation of a ring laser or microdisk laser, the rotational symmetry will be slightly broken due to inhomogeneities in the material or by imperfections of the manufacturing process [30,57]. While intuitively one would expect that a slight modification of the system should not change the structure of the lasing solutions, there is evidence that this symmetry breaking can have a strong effect on the lasing modes [57,58]. In order to better understand the impact of such a slight symmetry breaking on the stability of the SALT solutions, we analyze here a ring laser where the rotational symmetry is broken by a scatterer as depicted in Fig. 3(a). Similarly to the symmetric ring laser, such systems were previously investigated using simplified models and exhibited unstable or even chaotic behavior [45].

Since the inhomogeneity in this system breaks the rotational symmetry, solving Eq. (6) for the inactive system will not produce any traveling-wave solutions. Instead, standing-wave solutions similar to those found in the completely symmetric system are found. But while the standing-wave solutions of the symmetric system always occurred in degenerate pairs, breaking the symmetry lifts the degeneracy such that the new modes slightly differ in their complex frequencies $\bar{\omega}_i$. Therefore, they will neither possess exactly the same lasing frequency, nor will they reach the lasing threshold at exactly the same same pump strength D_0. Since the frequency splitting does not fulfill the stationary inversion approximation for realistic values of $\gamma_\parallel$, a possible two-mode solution cannot be described by SALT (at least not without an explicit stability analysis).

In our analysis we consider gain parameters that only support the lasing action of a single pair of such modes (here located at $\bar{\omega}_i \approx 62$) such that only the single-mode solutions of SALT seem viable candidates for steady-state lasing. These single-mode SALT solutions are shown in Fig. 3(b) in the form of their frequency dependence on the pump strength D_0. In particular, the two single-mode solutions of SALT corresponding to the pair of nearly degenerate resonator modes are shown as mode A and B. When tracking mode A from its threshold while increasing the pump strength, it shows the following behavior: At $D_0 \approx 0.0015$ the standing-wave single-mode solution A becomes active and the system starts lasing [see Fig. 3(b)]. At this pump value the mode is stable, both according to the traditional SALT criterion for stability as well as in the linear stability calculations. However, a very small increase of the pump strength brings the eigenvalue $\bar{\omega}_i$ of the second mode B of this near-degenerate pair to the real axis and thus renders the single-mode solution unstable (again, according to both criteria). Whether a stable two-mode

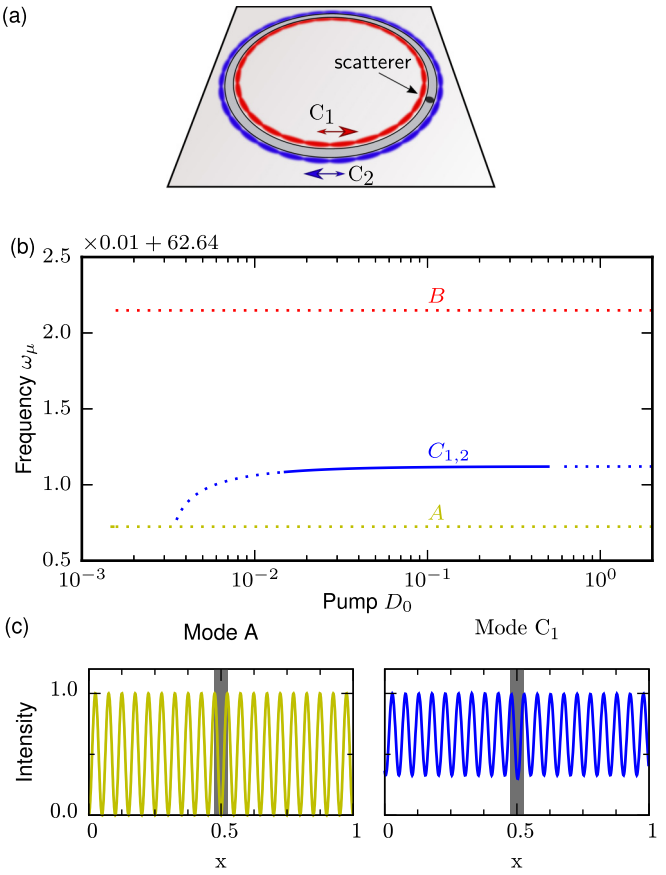

FIG. 3. (Color online) Results for a ring laser system as in Fig. 1 with $\gamma_\parallel = 0.01$, but with an additional scatterer added with $l = 0.05$ and $\sqrt{\epsilon} = 1.05 + 0.0002i$. (a) Sketch of the system. (b) Frequencies of single-mode SALT solutions. It can be seen that the two degenerate modes of the symmetric system from Fig. 1 have split into modes A and B. Additionally, at $D_0 \approx 0.003$, two predominantly traveling-wave solutions C_1 and C_2 branch off from solution A. These two solutions are mirror-symmetric images of each other. Dotted lines mark unstable, solid lines mark stable solutions. (c) Intensity distribution of modes A and C_1 with the scatterer marked in gray. To better show the differences in the shape of the modes, both modes are normalized to a maximal intensity of 1. Mode A is shown directly at threshold ($D_0 \approx 0.0015$), mode C_1 at $D_0 = 0.1$. It can be seen that while A is a standing wave with minimal intensity 0 at the nodes, the predominantly traveling-wave C_1 features a non-vanishing intensity everywhere in the cavity. The stability of mode $C_{1,2}$ is studied in Fig. 4.

solution in this near-degenerate regime exists is a question that presently falls outside the scope of SALT (due to the nonstationary inversion) [39]. However, with the techniques presented above we can investigate the stability of a single-mode solution in the regime beyond the point where the second mode passes the instability threshold. For this purpose, we track each of the two modes A and B towards higher pump strength using the SALT equation Eq. (4) for each mode as if the other mode was not active. Using, in addition, the stability criterion from the previous section reveals that both solutions on their own remain unstable for higher values of the pump strength. We find, however, that a bifurcation occurs at $D_0 \approx 0.003$, at which two further single-mode SALT solutions

$C_{1,2}$ of Eq. (4) branch off from solution A. These new modes share the same frequency, which lies approximately in between the frequencies of the unstable modes A and B. To find these two modes one can, e.g., use a linear superposition of mode A and B at higher pump strengths as an initial guess for solving Eq. (4), similarly to the way the traveling-wave solutions of the symmetric ring laser can be expressed as linear superpositions of the standing-wave solutions.

By looking at the mode profiles of solutions $C_{1,2}$ [C_1 is shown in Fig. 3(c)], we observe that these modes are related to the traveling-wave solutions observed in the system with unbroken rotational symmetry. There, the two stable solutions were purely clockwise or counterclockwise traveling waves. Here, each of the modes $C_{1,2}$ still features a dominant contribution in one direction and is identical to the other mode when being reflected at the symmetry axis containing the scatterer ($x = 0.5$). The major difference to the solutions observed in the unbroken ring laser is that the solutions $C_{1,2}$ do not exist below a critical pump strength $D_{\text{crit}} \approx 0.003$, since the nonlinear term in Eq. (4) needs to be strong enough to compensate for the frequency splitting between the two modes. The fact that the nonlinear term is responsible for compensating the frequency difference between the two nearly degenerate modes was further investigated. We used a linear approximation to estimate the frequency shift experienced by the passive mode of the system that corresponds to the single-mode solution B as a consequence of the spatial hole burning from the active mode A. For this purpose, we modeled the change in the population inversion $\Delta D(x)$ as well as the resulting change in frequency $\Delta\tilde{\omega}_B$ of the passive mode as a linear function of the pump strength D_0. The estimate predicted the two modes to share their frequency at a value of $D_0 \approx 0.30$, which is very close to the point $D_0 \approx 0.33$, where the solutions $C_{1,2}$ really emerge. The remaining small discrepancy can be attributed to the inaccuracy of the employed approximations.

Next, we check the stability of the mode pair $C_{1,2}$. First of all we recall that using the traditional SALT criterion Eq. (8) (which is not applicable here), one would find that the solutions $C_{1,2}$ are never stable. However, both the results of the FDTD calculations as well as the linear stability calculations do show that these modes are stable in well-defined limits. These limits are indicated in Fig. 4, where the stability of the single-mode solutions are depicted as obtained from both methods under variation of the pump strength D_0 as well as of the relaxation rate of the inversion $\gamma_\parallel$. As discussed in the above paragraph, there is a small region of stability for very low values of pump strength D_0 where mode A is stable. Of more interest, however, is the large region of stable lasing for modes $C_{1,2}$ which opens up at the critical pump strength $D_{\text{crit}} \approx 0.003$ (green region in Fig. 4) and which is similar to the one observed for the fully symmetric ring laser (Fig. 1).

Altogether, the results of the linear stability analysis are in excellent agreement with the findings of the time-dependent simulations of the MB equations, as can be seen both in Figs. 1(b) and 4. The linear stability analysis thus proves to be a reliable tool to classify the stability of SALT solutions and can therefore be used even for systems where verifying the results through time-dependent simulations is not feasible. This is, in particular, the case for higher dimensional systems, such as the microdisk system analyzed in the next section, where time-dependent simulations for a large range of parameters is computationally very demanding.

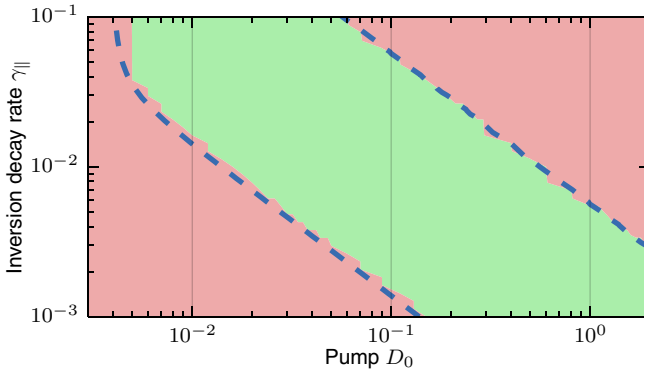

FIG. 4. (Color online) Stability of the SALT solution for the broken-symmetry ring laser shown in Fig. 3. The analyzed solution is the one marked as branch $C_{1,2}$ in Fig. 3(b). While the shape of the stability region is very similar to the one observed in Fig. 1, the broken-symmetry system requires a minimal pump strength D_0 to compensate for the frequency splitting of the nearly degenerate modes before a stable predominantly traveling-wave solution can emerge.

VI. EXAMPLE 3: 2D MICRODISK LASER WITH WEDGE

Next, we will extend our results to a two-dimensional system, where full time-dependent simulations become impractical for the required range of parameters, but the linear stability analysis can still be easily performed to justify the stability of the SALT solutions. The system we will consider is a perturbed 2D microdisk laser where the cavity is slightly deformed by cutting a small wedge into the disk [see arrow and white outline in Fig. 5(a)]. In analogy to the scatterer for the 1D ring laser, the wedge has the effect that the two originally degenerate threshold modes of the microdisk split (here the frequency splitting $\Delta\omega \approx 1.4 \times 10^{-3}$). Hence, the multimode condition $\gamma_\parallel \ll \Delta\omega$ cannot be satisfied for reasonable values of $\gamma_\parallel$ such that a two-mode solution does not fulfill the SIA and the traditional SALT algorithm cannot be applied.

The strategy to find the single-mode SALT solutions is a bit more sophisticated as compared to the 1D system. We start with the threshold modes A and B corresponding to the nearly degenerate resonances of the unpumped system and track them while gradually increasing the pump strength D_0 [see Fig. 5(b)]. Mode B has a lower threshold and is stable in a tiny pump region starting from its threshold at $D_0 \approx 0.0771$ up to about 0.0777. The corresponding stable parameter region for mode B, shown in the stability diagram in Fig. 5(c) by the green region on the very left of the figure, depends on both the pump strength D_0 and on $\gamma_\parallel$. After mode B has become unstable the mode is tracked further (neglecting the presence of mode A whose resonance eigenvalue has meanwhile also crossed the real axis). At $D_0 \approx 0.124$ a pair of solutions $C_{1,2}$ branches off from mode B. Whereas mode B and mode A feature a perfect even and odd symmetry with respect to the x axis (i.e., the symmetry axis of the system), the solutions $C_{1,2}$ do not possess this symmetry, but rather are mirror images of each other [compare mode profiles of modes B and C_1 in

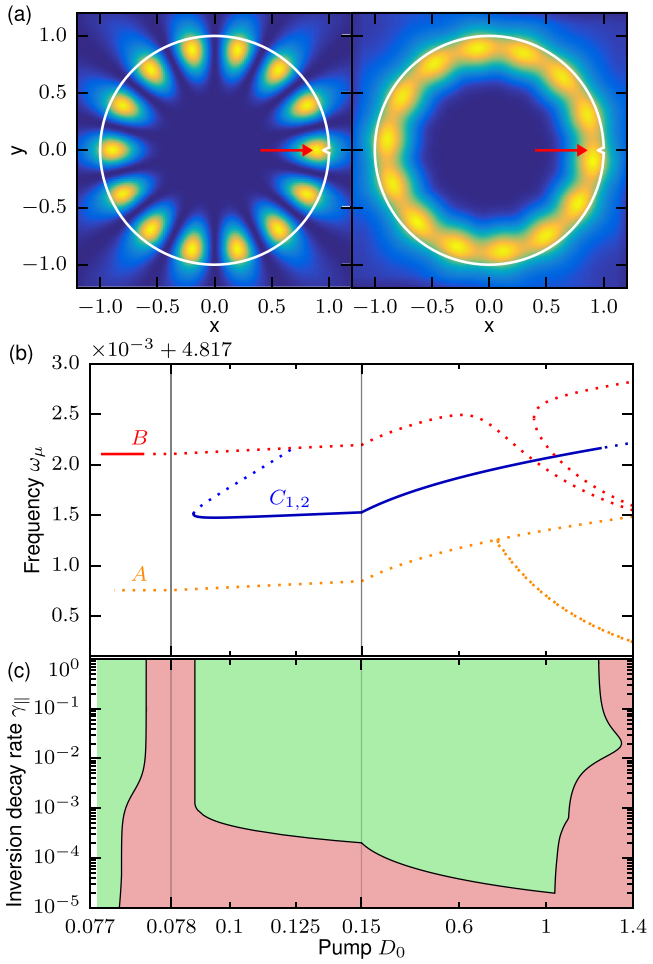

FIG. 5. (Color online) Single-mode lasing states for a 2D cavity with a wedge. The disk has a radius of 1, a refractive index of $n = 2 + 0.01i$, and the wedge on the right side of the disk has a depth of 0.05 and a width of 0.05. The gain parameters are $\omega_a = 4.83$ and $\gamma_\perp = 0.1$. (a) The cavity is outlined in white with arrows marking the position of the wedge. The spatial intensity pattern of two stable single-mode solutions are shown. Left: Standing-wave mode B at pump strength $D_0 = 0.0773$ with regularly spaced nodes with intensity zero. Right: dominantly traveling-wave solution C_1 at pump strength $D_0 = 0.15$. (b) Laser frequencies of single-mode solutions to the SALT Eq. (4). Curves A (orange) and B (red) correspond to two standing-wave solutions, which have even and odd symmetry with respect to the x axis. The two modes represented by curve $C_{1,2}$ (blue) feature a broken symmetry, but are mirror-symmetric to each other. Solid (dotted) lines denote a stable (unstable) solution for $\gamma_\parallel = 0.01$. Note that the pump axis is separated into three regions of different linear scaling for the sake of clarity. (c) Stability diagram of the single-mode solutions shown in (b) with respect to the pump strength D_0 and the relaxation rate of the inversion, $\gamma_\parallel$. The color coding is as in Fig. 1(c) except that the stability is here solely determined by the linear stability analysis.

Fig. 5(a)]. In fact, the symmetry of the system is spontaneously broken when either of these modes are lasing, a phenomenon that has been previously observed in simulations as well as in experiments [5].

In contrast to mode B, mode A is never a stable laser mode since it has a higher lasing threshold. At $D_0 \approx 0.8$ both (unstable) modes A and B feature two further branches. These can be understood as follows: Since the wedge of the two-dimensional cavity only represents a small perturbation to the system, the symmetry with respect to the y axis is only slightly broken, and, hence, modes A and B are nearly symmetric with respect to this axis [see left panel of Fig. 5(a) for the intensity pattern of mode B]. At $D_0 \approx 0.8$, this near symmetry is no longer realized. However, since the modes have never been fully symmetric, there is not a single point at which the symmetry breaks, but rather a smooth transition (as compared, e.g., to the symmetry-breaking transition with respect to the x axis at $D_0 \approx 0.124$). For mode B, this smooth transition is clearly visible in Fig. 5(b). For mode A this transition occurs in a much smaller pump interval, since mode A has a node directly located at the wedge of the 2D cavity and its symmetry is therefore only very slightly distorted.

To obtain modes $C_{1,2}$, we need to track them backwards in pump strength starting at the branching point at $D_0 \approx 0.124$ [see Fig. 5(b)]. Reducing the pump strength further, we observe that a sharp bend occurs in the frequency dependence of these two modes at $D_0 \approx 0.86$, where each of the modes $C_{1,2}$ has evolved into a dominantly traveling-wave mode [see right panel of Fig. 5(a)], similar to the nearly degenerate 1D ring laser. Note that the small contribution traveling in the clockwise direction can be observed as a modulation in the intensity pattern. Beyond this turning point, modes $C_{1,2}$ become stable in a large region of parameters D_0 and $\gamma_\parallel$ as depicted by the central green area in the stability diagram in Fig. 5(c). The easiest way to find the branch $C_{1,2}$ numerically is to sum the fields of modes A and B with an additional relative phase of $\pi/2$ at a pump strength $D_0 > 0.86$ and use this as a guess for the nonlinear solver to converge towards one of the dominantly traveling-wave modes. The solution can then be tracked to uncover the whole branch of modes $C_{1,2}$. Using similar superpositions of already known modes as starting point for the nonlinear solver, we found several more branches of nonlinearly induced single-mode SALT solutions within the plotted frequency range, albeit none of them are stable [these branches are not shown in Fig. 5(c)].

The traveling-wave solutions $C_{1,2}$ only remain stable until a pump strength of $D_0 \approx 1.3$. Here, the single-mode SALT solution becomes unstable due to the fact that an additional mode would start to lase. We also find that for values of $\gamma_\parallel < 2 \times 10^{-5}$ the modes $C_{1,2}$ are never stable, which highlights again how important it is to take into account the value of $\gamma_\parallel$ for assessing the stability of a SALT mode. Traditionally in SALT single-mode lasing solutions were implicitly considered as stable (without considering $\gamma_\parallel$) [17,22], but these single-mode solutions were always only identified for the case where only a single one of the eigenvalues $\bar{\omega}_i$ of Eq. (7) has a non-negative imaginary part. Our results show that single-mode SALT solutions can also exist for the case of multiple eigenvalues $\bar{\omega}_i$ featuring a non-negative imaginary part. In this new situation, a stability analysis is, however, indispensable for correctly interpreting the solutions of the SALT equation. When the results of the stability analysis are taken into account, the SALT equation allows us to accurately describe the steady state of these systems without requiring any time-dependent simulations.

VII. CONCLUSION

In this work we demonstrate that SALT can be used to describe the single-mode lasing regime of resonators with degenerate or near-degenerate mode pairs. Our approach builds on a careful tracking of SALT modes in the nonlinear lasing regime together with a linear stability analysis to judge the validity of the resulting solutions. The accuracy of the stability analysis itself was tested by a comparison with full time-dependent simulations based on the Maxwell-Bloch equations, which shows excellent agreement in all cases.

Our approach is ideally suited to treat microdisk whispering-gallery-mode lasers, which were previously difficult to simulate with SALT and often only accessible through time-dependent simulations or through strongly simplified models. Generally speaking, our work paves the way to study interesting nonlinear phenomena, such as bifurcating solutions, etc., within the efficient framework of SALT.

One obvious direction for further study is the generalization of our stability analysis to systems in the multimode lasing regime, which will be the aim of a subsequent paper [39].

ACKNOWLEDGMENTS

The authors acknowledge fruitful discussions with C. Abert, S. Esterhazy, T. Hisch, and H. E. Türeci. Financial support by the Vienna Science and Technology Fund (Austria), MA09-030 (LICOTOLI) and Austrian Science Fund (Austria), SFB NextLite F49-P10 is gratefully acknowledged. The computational results presented have been achieved using the Vienna Scientific Cluster (VSC).

APPENDIX: DERIVATION OF THE LINEAR STABILITY ANALYSIS

We start from a solution $\{E_1(x),\omega_1\}$ of the SALT Eq. (4) at a given pump strength D_0. From this, one can construct the polarization P_1 and inversion D that show up in the MB Eqs. (4) via

$$D(x) = \frac{D_0}{1+|\Gamma_1 E_1(x)|^2}, \tag{A1}$$

$$P_1(x) = \Gamma_1 D(x) E_1(x). \tag{A2}$$

Using these quantities, we insert the ansatz (9) into the MB Eqs. (1). Using the fact that $(E_1 e^{-i\omega_1 t}, P_1 e^{-i\omega_1 t}, D)$ is a solution of the MB equations, we linearize the equations with respect to the perturbations. This results in the following partial differential equations for the perturbations of the electric field, the polarization, and the inversion:

$$\epsilon\,\delta\ddot{E} = \nabla^2\delta E - \delta\ddot{P} + \omega_1^2(\delta P + \epsilon\,\delta E) + 2i\omega_1(\delta\dot{P} + \epsilon\,\delta\dot{E}), \tag{A3}$$

$$\delta\dot{P} = (i(\omega_1-\omega_a)-\gamma_\perp)\delta P - i\gamma_\perp(E\,\delta D + \delta E\, D), \tag{A4}$$

$$\delta\dot{D} = -\gamma_\parallel\,\delta D + \frac{i\gamma_\parallel}{2}(\delta E\, P_1^* + E_1\,\delta P^* - \delta E^* P_1 - E_1^*\,\delta P). \tag{A5}$$

While this system of equations is linear in the perturbation, it includes the terms δP^* and δE^*, which cannot be expressed as a linear combination of $\delta P, \delta E, \delta D$. In order to produce a completely linear system of equations, we therefore split the two complex fields and corresponding perturbations, as well as a possibly complex dielectric function ε into their respective real and imaginary parts and consequently split Eqs. (A3) and (A4) into four real equations. This yields a linear system of five equations with purely real terms. These correspond to the five independent fields $\mathrm{Re}(\delta E)$, $\mathrm{Im}(\delta E)$, $\mathrm{Re}(\delta P)$, $\mathrm{Im}(\delta P)$, δD, which for convenience we can summarize as a single vector field $\vec{F}$.

In order to analyze if a solution E_1 of the SALT equation (4) is stable we need to check if a perturbation exists which does not relax back to the stable solution. Hence, we make an ansatz of the form $\vec{F}(x,t) = \vec{F}(x)e^{\sigma t}$ which yields

$$\begin{aligned}
(\delta P_r - \epsilon_i\delta E_i + \epsilon_r\delta E_r)\sigma^2 + 2(\delta P_i + \epsilon_i\delta E_r + \epsilon_r\delta E_i)\omega_1\,\sigma - (\delta P_r - \epsilon_i\delta E_i + \epsilon_r\delta E_r)\,\omega_1^2 - \nabla^2\delta E_r &= 0,\\
(\delta P_i + \epsilon_i\delta E_r + \epsilon_r\delta E_i)\sigma^2 - 2(\delta P_r - \epsilon_i\delta E_i + \epsilon_r\delta E_r)\omega_1\sigma - (\delta P_i + \epsilon_i\delta E_r + \epsilon_r\delta E_i)\omega_1^2 - \nabla^2\delta E_i &= 0,\\
\delta P_r\sigma + \gamma_\perp\left(\delta P_r - D\delta E_i - \delta D E_i^1\right) + (\omega_1-\omega_a)\delta P_i &= 0,\\
\delta P_i\sigma + \gamma_\perp\left(\delta P_i + D\delta E_r + \delta D E_r^1\right) - (\omega_1-\omega_a)\delta P_r &= 0,\\
\delta D\sigma + \gamma_\parallel\left(\delta D + P_r^1\delta E_i + \delta P_r E_i^1 - \delta E_r P_i^1 - E_r^1\delta P_i\right) &= 0,
\end{aligned} \tag{A6}$$

where we have abbreviated $\mathrm{Re}(\cdot)$ and $\mathrm{Im}(\cdot)$ through the subindices r and i, respectively. In addition we need to impose boundary conditions for the perturbation δE. For the periodic 1D ring laser we can simply assume periodic boundary conditions, i.e., $\delta E(x_{\mathrm{left}}) = \delta E(x_{\mathrm{right}})$ and for the 2D system $\vec{\nabla}\delta E \overset{r\to\infty}{=} i(\omega_1 - i\sigma)\delta E\,\hat{e}_r$. In a next step Eqs. (A6) are discretized using a suitable discretization scheme [22] which leads to a quadratic eigenvalue problem that can easily be linearized. In our calculations we have chosen the finite element framework FEniCS [59] for discretizing Eqs. (A6) and used a perfectly matched layer for imposing the outgoing boundary conditions in the 2D case. For solving the linearized quadratic eigenvalue problem we have used SLEPc [60].

[1] K. J. Vahala, Nature (London) **424**, 839 (2003).
[2] H. Cao and J. Wiersig, Rev. Mod. Phys. **87**, 61 (2015).
[3] J. U. Nöckel and A. D. Stone, Nature (London) **385**, 45 (1997).
[4] C. Gmachl, F. Capasso, E. E. Narimanov, J. U. Nöckel, A. D. Stone, J. Faist, D. L. Sivco, and A. Y. Cho, Science **280**, 1556 (1998).
[5] T. Harayama, T. Fukushima, S. Sunada, and K. S. Ikeda, Phys. Rev. Lett. **91**, 073903 (2003).
[6] M. Lebental, J. S. Lauret, R. Hierle, and J. Zyss, Appl. Phys. Lett. **88**, 031108 (2006).
[7] Q. Song, W. Fang, B. Liu, S.-T. Ho, G. S. Solomon, and H. Cao, Phys. Rev. A **80**, 041807 (2009).
[8] Q. J. Wang, C. Yan, N. Yu, J. Unterhinninghofen, J. Wiersig, C. Pflügl, L. Diehl, T. Edamura, M. Yamanishi, H. Kan, and F. Capasso, Proc. Natl. Acad. Sci. USA **107**, 22407 (2010).
[9] J. Yang, S.-B. Lee, S. Moon, S.-Y. Lee, S. W. Kim, T. T. A. Dao, J.-H. Lee, and K. An, Phys. Rev. Lett. **104**, 243601 (2010).
[10] F. Albert, C. Hopfmann, A. Eberspächer, F. Arnold, M. Emmerling, C. Schneider, S. Höfling, A. Forchel, M. Kamp, J. Wiersig, and S. Reitzenstein, Appl. Phys. Lett. **101**, 021116 (2012).
[11] B. Peng, Ş. K. Özdemir, S. Rotter, H. Yilmaz, M. Liertzer, F. Monifi, C. M. Bender, F. Nori, and L. Yang, Science **346**, 328 (2014).
[12] M. Brandstetter, M. Liertzer, C. Deutsch, P. Klang, J. Schöberl, H. E. Türeci, G. Strasser, K. Unterrainer, and S. Rotter, Nat. Commun. **5**, 4034 (2014).
[13] H. Haken and H. Sauermann, Z. Phys. **173**, 261 (1963).
[14] W. E. Lamb, Phys. Rev. **134**, A1429 (1964).
[15] R. Lang, M. O. Scully, and W. E. Lamb, Phys. Rev. A **7**, 1788 (1973).
[16] H. Haken, *Laser Light Dynamics* (North-Holland, Amsterdam, 1986), Vol. II.
[17] H. E. Türeci, A. D. Stone, and B. Collier, Phys. Rev. A **74**, 043822 (2006).
[18] L. Ge, R. J. Tandy, A. D. Stone, and H. E. Türeci, Opt. Express **16**, 16895 (2008).
[19] H. E. Türeci, A. D. Stone, L. Ge, S. Rotter, and R. J. Tandy, Nonlinearity **22**, C1 (2009).
[20] L. Ge, Y. D. Chong, and A. D. Stone, Phys. Rev. A **82**, 063824 (2010).
[21] A. Cerjan and A. D. Stone, Phys. Rev. A **90**, 013840 (2014).
[22] S. Esterhazy, D. Liu, M. Liertzer, A. Cerjan, L. Ge, K. G. Makris, A. D. Stone, J. M. Melenk, S. G. Johnson, and S. Rotter, Phys. Rev. A **90**, 023816 (2014).
[23] A. Pick, A. Cerjan, D. Liu, A. W. Rodriguez, A. D. Stone, Y. D. Chong, and S. G. Johnson, Phys. Rev. A **91**, 063806 (2015).
[24] H. E. Türeci, L. Ge, S. Rotter, and A. D. Stone, Science **320**, 643 (2008).
[25] M. Liertzer, L. Ge, A. Cerjan, A. D. Stone, H. E. Türeci, and S. Rotter, Phys. Rev. Lett. **108**, 173901 (2012).
[26] M. Chitsazi, S. Factor, J. Schindler, H. Ramezani, F. M. Ellis, and T. Kottos, Phys. Rev. A **89**, 043842 (2014).
[27] Y. D. Chong, L. Ge, H. Cao, and A. D. Stone, Phys. Rev. Lett. **105**, 053901 (2010).
[28] W. Wan, Y. Chong, L. Ge, H. Noh, A. D. Stone, and H. Cao, Science **331**, 889 (2011).
[29] T. Hisch, M. Liertzer, D. Pogany, F. Mintert, and S. Rotter, Phys. Rev. Lett. **111**, 023902 (2013).
[30] S. F. Liew, B. Redding, L. Ge, G. S. Solomon, and H. Cao, Appl. Phys. Lett. **104**, 231108 (2014).
[31] D. Gagnon, J. Dumont, J.-L. Déziel, and L. J. Dubé, J. Opt. Soc. Am. B **31**, 1867 (2014).
[32] H. Zeghlache, P. Mandel, N. B. Abraham, L. M. Hoffer, G. L. Lippi, and T. Mello, Phys. Rev. A **37**, 470 (1988).
[33] H. Risken and K. Nummedal, Phys. Lett. **A26**, 275 (1968).
[34] S.-L. Chua, Y. Chong, A. D. Stone, M. Soljacic, and J. Bravo-Abad, Opt. Express **19**, 1539 (2011).
[35] A. Cerjan, Y. Chong, L. Ge, and A. D. Stone, Opt. Express **20**, 474 (2012).
[36] The restriction to TM modes is only due to the fact that this simplifies the equations. However, the results presented in this work equally apply if one uses the full three-dimensional MB, where E^+, P^+ are vector quantities.
[37] J.-P. Berenger, J. Comput. Phys. **114**, 185 (1994).
[38] As discussed in [22] further conditions come into play for the "bad cavity limit," which, however, we do not consider for the systems shown in this paper.
[39] S. Burkhardt *et al.* (unpublished).
[40] L. A. Lugiato, L. M. Narducci, and M. F. Squicciarini, Phys. Rev. A **34**, 3101 (1986).
[41] D. M. J. V. Moloney, H. Adachihara, and A. Newell, in *Chaos, Noise and Fractals*, Malvern Physics Series, edited by E. Pike and L. Lugiato (Taylor & Francis, London, 1987), pp. 137–187.
[42] G. Grynberg, E. L. Bihan, P. Verkerk, P. Simoneau, J. Leite, D. Bloch, S. L. Boiteux, and M. Ducloy, Opt. Commun. **67**, 363 (1988).
[43] G. Giusfredi, J. F. Valley, R. Pon, G. Khitrova, and H. M. Gibbs, J. Opt. Soc. Am. B **5**, 1181 (1988).
[44] L. Lugiato, F. Prati, L. Narducci, and G.-L. Oppo, Opt. Commun. **69**, 387 (1989).
[45] *Principles of Laser Dynamics*, edited by Y. Khanin (Elsevier Science, New York, 1995), Chapter 5.
[46] H. E. Tureci and A. D. Stone, Proc. SPIE **5708**, 255 (2005).
[47] G. V. der Sande, L. Gelens, P. Tassin, A. Sciré, and J. Danckaert, J. Phys. B **41**, 095402 (2008).
[48] S. Sunada, T. Harayama, K. Arai, K. Yoshimura, K. Tsuzuki, A. Uchida, and P. Davis, Opt. Express **19**, 7439 (2011).
[49] S. T. Kingni, G. V. der Sande, L. Gelens, T. Erneux, and J. Danckaert, J. Opt. Soc. Am. B **29**, 1983 (2012).
[50] M. V. Danileiko, A. L. Kravchuk, V. N. Nechiporenko, A. M. Tselinko, and L. P. Yatsenko, Sov. J. Quantum Electron. **16**, 1420 (1986).
[51] K. Yee, IEEE Trans. Antennas Propag. **14**, 302 (1966).
[52] B. Bidégaray, Numer. Methods Partial Differ. Equations **19**, 284 (2003).
[53] The only difference between the MB Eqs. (1) and the ones used for the time-dependent simulations is that within the latter, losses are represented by an additional term describing the electrical conductivity of the medium instead of a complex dielectric function (see, e.g., [16]). Using the conductivity $\sigma = \mathrm{Im}(\epsilon)\omega_1$, this results in identical single-mode lasing behavior.
[54] We alternatively analyzed the situation when the simulation was not initialized in the state obtained from the SALT solution but in an arbitrary initial state instead. If the parameters of the system were such that the SALT solution was stable (see Fig. 1), the system would usually converge to the SALT solution over time.

In the region close to the border between stable and unstable solution, the system only converged to the SALT solution for certain initial conditions, hinting at the existence of a second stable non-steady-state solution.

[55] The instability at higher values of D_0 and $\gamma_\parallel$, which is not present in the model by Zeghlache *et al.* [32], involves other resonances of the passive cavity. These resonances have little influence in lasers with sufficiently large mode spacing ($\Delta\omega \gg \gamma_\perp$), but play an important role in the systems we analyze, where the mode spacing $\Delta\omega$ is comparable to $\gamma_\perp$.

[56] Y. Saad, *Numerical Methods for Large Eigenvalue Problems* (Halsted, New York, 1992).

[57] S. F. Liew, L. Ge, B. Redding, G. S. Solomon, and H. Cao, Phys. Rev. A **91**, 043828 (2015).

[58] J. Wiersig, Phys. Rev. A **84**, 063828 (2011).

[59] A. Logg, K.-A. Mardal, and G. Wells, eds., *Automated Solution of Differential Equations by the Finite Element Method*, Lecture Notes in Computational Science and Engineering Vol. 84 (Springer, Berlin, Heidelberg, 2012).

[60] V. Hernandez, J. E. Roman, and V. Vidal, ACM Trans. Math. Softw. **31**, 351 (2005).